

The virtual AirDyn: a simulation technique for evaluating the aerodynamic impact of ship superstructures on helicopter operations

C. H. Kääriä

School of Engineering
University of Liverpool
Liverpool, UK

J. S. Forrest

Prism Defence
Adelaide, Australia

I. Owen

iowen@lincoln.ac.uk

School of Engineering
University of Lincoln
Lincoln, UK

ABSTRACT

This paper describes a simulation technique that has been developed to quantify the unsteady forces and moments that are imposed onto a maritime helicopter by a ship's airwake during a deck landing. An unsteady CFD-generated airwake, created using a CAD model of the ship, is integrated with a flight dynamics model of a helicopter. By holding the helicopter at a fixed position in the airwake it is possible to quantify the unsteady forces and moments imposed on the aircraft. The technique is therefore a software-based airwake dynamometer, and has been called the virtual AirDyn. As well as determining the mean loads, from consideration of the unsteady loads in the closed-loop pilot response frequency range of 0.2-2Hz it is also possible to quantify the magnitude of the unsteady disturbance in each axis. The loads are also indicators of the control activity the pilot would have to exert to maintain aircraft position and attitude. By placing the virtual AirDyn at different positions around the landing deck in different wind conditions, it is able to quantify the effect of the airwake on the mean and unsteady loads. The quantified loads can be explained by examining the CFD-generated flow field, and the geometric features on the ship's superstructure that gave rise to them can be identified. The virtual AirDyn is therefore a tool that can be used to evaluate and inform ship design for maritime helicopter operations.

NOMENCLATURE

b	width of landing deck, m
C_T	non-dimensional thrust coefficient
h	height of hangar, m
l	length of landing deck, m
u, v, w	velocity components in x, y, z , ms^{-1}
x, y, z	distances measured from deck centreline and hangar face, defined in Fig. 2, m
V_∞	freestream velocity, ms^{-1}

1.0 INTRODUCTION

Landing a maritime helicopter to the flight deck of a ship is a difficult and demanding task for even the most experienced pilots. As well as operating to a restricted landing area on a pitching, rolling and heaving ship, the pilot must also contend with the presence of a highly unsteady air flow over the flight deck. This phenomenon, known as the ship's 'airwake', is caused by the air flowing over and around the ship's superstructure as a result of the combined effect of the prevailing wind and the forward motion of the ship.

Although the helicopter is the ship's most potent asset, the geometry of the superstructure is not designed with the airwake in mind, largely because the aerodynamic design guidance is not available. Over recent years there has been significant collaborative international research into the 'ship-helicopter dynamic interface': the region where the unsteady and irregular motions of both the landing deck and the airflow combine to create a major challenge for the pilot and the helicopter's operational envelope. Flight deck aerodynamics has been investigated using techniques such as flow visualisation⁽¹⁻⁵⁾, anemometry⁽³⁻⁷⁾, and computational fluid dynamics (CFD)⁽⁸⁻¹¹⁾. As a result, the key features of the airwake are now relatively well understood⁽¹²⁾. The superstructure is a collection of bluff bodies and its sharp edges lead to flow separation and the formation of strong shear layers and vortices, causing large spatial and temporal gradients in the air flow over the flight deck. The degree of unsteadiness in the airwake will also be affected by large-scale geometric features such as masts, radar domes and weapon systems and the nature and severity of the airwake will vary significantly with wind-over-deck (WOD) speed and direction.

As the pilot moves the helicopter through the airwake during an approach to landing, the highly unsteady airflow causes large fluctuations in the aerodynamic loading on the aircraft's fuselage and rotors making it very difficult for the pilot to maintain position and attitude. Unsteady loads in the frequency range 0.2-2Hz are particularly difficult for the pilot to contend with: forces and moments with frequencies above this range are damped by the inertia of the aircraft, while loads with frequencies below the range can be overcome by the pilot through the aircraft's controls. Disturbances with frequencies between 0.2 and 2Hz are considered to be in the closed-loop pilot response frequency range^(13,14). When the ship's airwake imposes significant loads at these frequencies, if the pilot workload required to maintain aircraft stability is so high, and if the pilot's spare capacity to perform ancillary tasks is so reduced, the landing is deemed unsafe. Such conditions are then considered outside the safe operational limits of the ship-helicopter combination in question.

As well as workload, the spare control margins available to the pilot throughout an operation are also an important factor to consider when establishing safe operational envelopes. If the pilot is required to move a control inceptor to within 10% of its maximum travel during a landing task then the capability to respond to large disturbances in that axis is severely compromised. The

reduction in control margin can therefore lead to an operational limit being imposed because the pilot's ability to maintain control of the aircraft and to deal with strong gusts encountered in the unsteady airwake is reduced.

Recognising the need to develop techniques to evaluate the effect of ship superstructure geometry on helicopter flight handling qualities and pilot workload, Wang *et al*⁽¹⁵⁾ developed an instrument which they called the 'AirDyn'. The instrument is a model-scale helicopter, with a motored main rotor, mounted onto a six-axis force block so that it measures dynamic loads (lift, drag, side) and moments (pitch, roll, yaw). When immersed in the wake of a model ship it measures the unsteady aerodynamic loads being imposed on the helicopter by the airwake and is therefore an Airwake Dynamometer – hence the AirDyn. The model scale of the AirDyn and the associated ship geometry was 1/54th of full scale and Kääriä *et al*⁽¹⁶⁾ used the instrument to evaluate the airwake of a simplified ship and to explain some control issues that maritime pilots often encounter, such as 'thrust deficit' behind the hangar in headwinds and the 'pressure wall' in oblique winds. In Ref. 17 Kääriä *et al* used the AirDyn to evaluate the effects of different superstructure modifications on helicopter loading and showed that relatively simple modifications could have a significant impact in reducing the unsteady loads.

A useful outcome from the work reported in Refs 15-17 is the observation that the average aerodynamic loads are largely responsible for using up the helicopter's control margins, and the unsteady components are largely responsible for pilot workload. Similar observations were made by Forrest *et al* who conducted simulated deck landings in a motion base flight simulator where a pilot 'flew' a Lynx helicopter to the deck of a Type 23 frigate⁽¹⁸⁾. For example, a strong oblique wind across the landing deck will cause the pilot to use lateral cyclic to hold position, and pedal to counteract yaw; the stronger the wind the more the control margin is used up. If the oblique wind has significant unsteadiness, particularly in the 0.2-2Hz frequency range (at full-scale), it will cause considerable control movements and pilot workload. The combination of reduced control margin and increased pilot workload is a common reason for the ship-helicopter operating limit to be exceeded and for the pilot to abort the landing task.

The research reported in this paper takes the concept of the experimental AirDyn and, drawing on the simulation approach of Forrest *et al*⁽¹⁸⁾, it replaces the physical elements with software-based equivalents. The model helicopter is replaced by a full-scale flight dynamics model, the ship model is replaced by a full-scale CAD solid model, and CFD is used to create the ship airwake. The simulation technique is replicating the experimental AirDyn, and we have therefore called it the 'Virtual AirDyn'.

2.0 THE VIRTUAL AIRDYN

The helicopter flight dynamics model was developed in FLIGHTLAB, a commercially available software tool that provides a multi-body modelling and simulation environment⁽¹⁹⁾. Using FLIGHTLAB, complete rotorcraft simulations can be constructed from a library of pre-defined components⁽²⁰⁾. For the current work a FLIGHTLAB model of a helicopter having a conventional articulated main rotor with four blades was configured to be representative of a Sikorsky SH-60B Seahawk helicopter. The SH-60B, Fig. 1, is a maritime helicopter which is currently in service with several navies throughout the world; it is derived from the ubiquitous UH-60A Black Hawk utility helicopter. The SH-60B was selected because of the wide availability of engineering data for that type of helicopter in the open literature^(21,22). For a comparative study on the effects of ship geometry and airwake on the helicopter it is not critical which helicopter type is used, but it is important that it is a reliable model.



Figure 1. Sea-Hawk SH-60B helicopter.

The FLIGHTLAB model of the SH-60B comprises the following major subsystem components: (1) individual blade-element main-rotor model including look-up tables of non-linear lift, drag and pitching moment coefficients stored as functions of incidence and Mach number; (2) Bailey disk tail-rotor model, (3) finite-state Peters-He dynamic inflow model; (4) separate look-up tables for the fuselage, vertical tail and the port and starboard stabilator forces and moments stored as nonlinear functions of incidence and sideslip; (5) turbo-shaft engine model with a rotor-speed governor; (6) primary mechanical flight control system and stability augmentation system (SAS) models including sensor and actuator dynamics; and (7) a landing gear model to provide deck reaction cues on touchdown. Padfield⁽²³⁾ describes this level of modelling as medium fidelity, capable of simulating trim and primary-axis responses faithfully. Handling qualities characteristics are also generally well predicted using this type of flight dynamics model.

To create unsteady aerodynamic loads on the aircraft, it is clearly essential to generate an unsteady airwake and to accurately resolve the unsteady velocity components and flow structures. In a domain of this size the rational technique to apply is large eddy simulation (LES) as deployed by Thornber *et al*⁽⁹⁾ for computing the airwakes of two UK Royal Navy ships: a Type 23 frigate and a wave class auxiliary oiler. Their comparisons of the LES-generated velocity components and turbulent power spectra showed good agreement with experimental wind-tunnel data. In the study being reported here we chose to use the hybrid LES/RANS method of detached eddy simulation (DES) which is particularly well suited to ship airwake computations because in regions of interest where the accurate capture of turbulent features is important, turbulence is explicitly resolved by the grid (as long as mesh resolution is sufficiently fine); whereas in regions of irrotational flow away from the body of interest and close to walls, the standard SST $k-\omega$ RANS model is used. This leads to relatively modest computational requirements compared with LES, as it relaxes near-wall mesh requirements and allows large cells to be employed away from the ship. Using an unstructured mesh containing about 6 million cells, the computations were partitioned across 32 processors on a high performance computing cluster, taking about 60 hours to generate 30 seconds of full-scale airwake data. The computations were performed using the unstructured finite-volume code, FLUENT. Spatial discretisation of the convective terms was performed using the hybrid MUSCL scheme, with pressure-velocity coupling achieved using FLUENT's 'coupled' solver. A second-order implicit time-advancement scheme was employed for temporal discretisation, using 10 sub-iterations per time-step. The chosen time-step was set equal to $\Delta t^* = (\Delta t V)/b = 0.0075$, where b is the ship's beam. The computations were run for a flow time of 15 seconds to allow

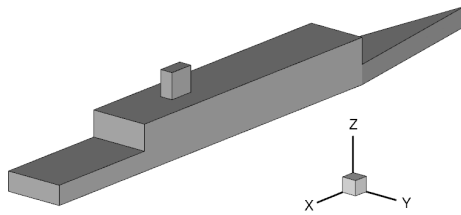


Figure 2. Simple frigate shape 2 (SFS2).

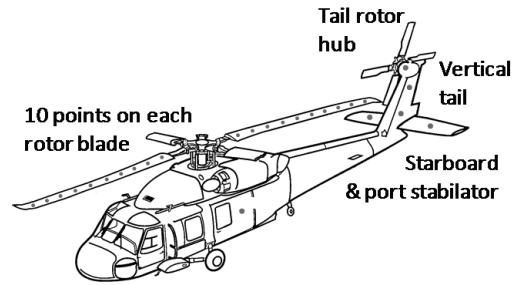


Figure 3. Location of airload computation points on the SH-60B helicopter model.

start-up transients to decay, before sampling was started.

The detail of the airwake generation method has been described in detail by Forrest and Owen⁽⁸⁾ and the computations have been extensively validated against model-scale and full-scale data, where it was shown that the spatial and temporal characteristics of the airwake are well modelled. The airwakes are created for a range of wind directions, usually from 90° starboard to 90° port, and typically for a wind strength of 40 knots. Both direction and speed are relative to the deck (i.e. wind-over-deck, WOD).

For this study the ship model we have chosen to use is the simple frigate Shape 2 (SFS2), shown in Fig. 2. SFS2 is a generic frigate shape created under the auspices of The Technical Cooperation Program (TTCP) as a means of comparing the numerous CFD and experimental studies of researchers from the member states. The SFS2 was chosen for this study because of its relatively simple geometry and flow features compared with more realistic frigate shapes. Future work will build on this study to investigate more realistic ship shapes, such as those modelled by Forerst and Owen⁽⁸⁾ and Thorber *et al.*⁽⁹⁾. A further benefit of using the SFS2 is the availability of high quality wind-tunnel data from experiments provided by the National Research Council of Canada (NRC), which has been used to validate the CFD airwakes used in this study. Comprehensive comparisons between CFD and experimental data can be found in the study by Forrest and Owen⁽⁸⁾ where very good agreement is demonstrated in terms of mean and unsteady velocity components around the flight deck, and in the turbulent power spectra.

The unsteady CFD airwake simulations produced large quantities of time-varying data for each of the three airwake velocity components, sampled at each point on an unstructured computational mesh at a rate of 80Hz. The data in this format was unsuitable for direct implementation into FLIGHTLAB. Instead, the data was first interpolated onto a structured orthogonal grid, so that it could be stored in look-up tables. Furthermore, to reduce the data storage burden, only every fourth time step was used (i.e. the data was down-sampled to 20Hz). The structured grid was designed to cover only the region around the ship where the helicopter is expected to operate during deck landings. A uniform grid spacing of 1m was selected, because this resolution compares well with the SH-60B main rotor diameter of approximately 16m. For the airwake model to influence the flying qualities of the simulated helicopter, the airwake velocity components must be converted into forces and moments, and applied at the helicopter model's centre of gravity. To accomplish this, local airwake velocity components are applied at a number of airload computation points (ACPs) distributed around the helicopter. A total of 46 ACPs were defined for the SH-60B model, as shown in Fig. 3. There is one ACP at the centre of each of the ten blade elements on each of the four main rotor blades, one at the tail rotor hub, two on the vertical tail surface, one each on the port and starboard stabilators and one at the aerodynamic centre of the fuselage.

Table 1
Collective and cyclic blade pitch angles

WOD angle	Collective pitch	Lateral cyclic	Longitudinal cycle
Headwind	15.25°	-2.50°	2.36°
Green 30	15.16°	-1.64°	3.05°

The Virtual AirDyn method requires the simulated helicopter to be held fixed in space and immersed in the ship airwake while measuring the unsteady forces and moments at the model's centre of gravity, just as they are in the experimental AirDyn. During a simulation run, at each time step, the spatial location of every ACP is computed relative to the ship. The resulting positions in x , y and z and the time, t , are then used to extract the local airwake velocity components, at each ACP, at that time from the airwake look-up tables using a four-dimensional interpolation algorithm. The airwake velocities are defined in ship axes, so for the fuselage, empennage (stabilators and vertical tail) and tail rotor hub, these velocities must be transformed into the helicopter body-fixed reference frame. A further conversion into local rotor blade co-ordinates is required for each ACP on the main rotor blades.

3.0 TEST PROGRAMME AND DATA ACQUISITION

This study has employed the use of naval terminology, such that 'green' and 'red' refer to the starboard and port sides of the ship respectively. Therefore a G30 wind denotes a WOD angle of thirty degrees from the longitudinal centreline of the ship, originating from the right hand side when looking towards the bow. In the discussions to follow, velocity and turbulence data is normalised by freestream velocity. Longitudinal, lateral and vertical spatial co-ordinates (x , y , z) are normalised by deck length (l), ship beam (b) and hangar height (h) respectively. The helicopter model was trimmed with an airspeed of 40kts at a wind direction consistent with the airwake WOD angle. The trim was required to reduce the effect of the lift imbalance between the advancing and retreating blades; the resulting collective and cyclic pitch angles are shown below in Table 1. These values were retained throughout the simulations at each test point.

The aircraft was then placed, in turn, at 49 points relative to the SFS2 flight deck as shown in Fig. 4. The rotor hub vertical (z) position was maintained at a constant height of 6.1m above the flight deck, which corresponds to the height of the top the hangar from the deck and is a typical height for the rotor head when the helicopter is translating across the landing deck. Once fixed at a particular test point, the model's translational and rotational degree of freedom states were disabled in FLIGHTLAB and the unsteady airwake was run for a period of thirty seconds; this procedure was performed for a headwind and G30 WOD azimuth. Any wind direction can be selected, provided the airwake for that angle has been computed, but for the purposes of this paper only these two wind directions were used.

Time-histories of the unsteady forces and moments at the model's centre of gravity were recorded for 30s. The data was time-averaged to enable comparisons of the mean aerodynamic loading characteristics between the test points and WOD conditions. The simulated unsteady aerodynamic loading characteristics were generated using the method adopted by Lee and Zan^(13,14) in their experimental investigations of the aerodynamic loading of a helicopter fuselage and rotor in a ship airwake. As discussed earlier, it is disturbances in the frequency range 0.2–2Hz which have the most significant impact on helicopter handling qualities and pilot workload⁽²⁴⁾. Therefore, when performing statistical

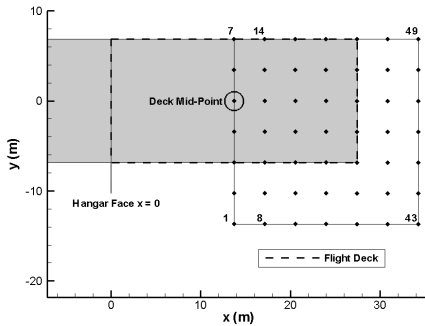


Figure 4. Locations of helicopter model centre of gravity in relation to the SFS2 flight deck.

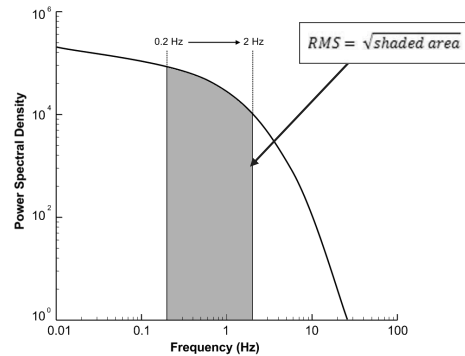


Figure 5. Closed-loop pilot response frequency bandwidth.

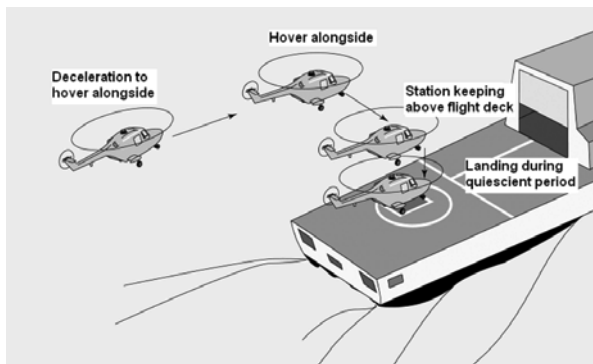


Figure 6. Final stages of the recovery of a Royal Navy helicopter to a single spot frigate.

analysis of unsteady loading, the usual definition of root-mean-square (RMS) of the deviations from the mean is not the ideal way to quantify the impact of the airwake as it includes fluctuations at frequencies outside the bandwidth known to be responsible for airwake-induced pilot workload. Instead, power spectral density (PSD) plots have been derived from the force and moment time-histories and the square root of the integral between the limits 0.2–2 Hz (shown schematically in Fig. 5) has been used as a measure of the RMS loading in this frequency bandwidth. This quantity will hereby be referred to as the RMS loading of the particular force or moment in question (e.g. RMS yawing moment). The RMS loading in each of the 6 degrees-of-freedom has been used to characterize the unsteady aerodynamic loading of the SH-60B as a result of the ship's airwake.

The unsteady aerodynamic loading data presented in this paper has been analysed in such a way that it relates to the standard UK Royal Navy landing approach technique (Fig. 6). A typical ship-helicopter landing operation comprises a series of mission task elements (MTEs) as follows:

1. Approach and port-side hover
2. Lateral translation
3. Station keeping over the flight deck
4. Vertical descent to landing spot

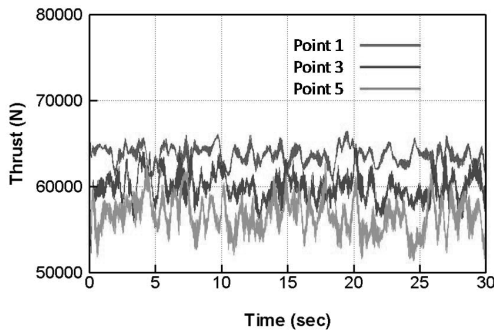


Figure 7. Time-histories of thrust in a headwind at points along the approximate path of the lateral translation MTE at $x/l = 0.5$.

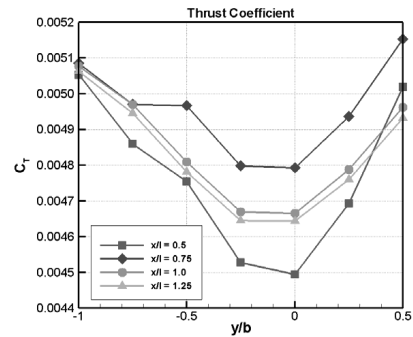


Figure 8. Time-averaged thrust coefficient in a headwind at various longitudinal locations.

The operation begins with an approach alongside the flight deck to a stabilised hover to the port side of the ship. The pilot then executes a lateral translation across the deck to a stabilised hover over the landing spot. The pilot then maintains station over the spot until there is a quiescent period in the ship's deck motion, before finally executing a descent to the flight deck. For the purposes of this study the landing spot is assumed to be on the centreline of the SFS2 at a longitudinal location halfway between the hangar face and the stern.

4.0 RESULTS AND DISCUSSION

As mentioned earlier, only two wind directions have been used in this study as this is sufficient to demonstrate the operation of the Virtual AirDyn. Similarly, the Virtual AirDyn is capable of quantifying both the mean and the RMS loads in all six axes, but only a selection of data will be presented.

4.1 Thrust characteristics in headwind

The time histories of thrust at the headwind condition for Points 1, 3 and 5 (identified in Fig. 4) are shown in Fig. 7. These points are on a lateral line aligned with the landing spot, which corresponds to the approximate path of the lateral translation MTE as executed in a port-side approach deck landing. Figure 7 shows that as the aircraft model translates from the port-side to the centreline of the ship, moving from the freestream to a location fully immersed in the airwake, mean thrust decreases and the magnitude of thrust fluctuations increases.

Figure 8 shows the time-averaged thrust coefficient (C_T) plotted against lateral deck position for various distances from the hangar face. At the longitudinal location $x/l = 0.5$, aligned with the landing spot, there is a reduction in thrust of approximately 11% as the aircraft moves laterally from the freestream to the ship centreline. This trend is consistent with the experimental study of rotor thrust in a ship's airwake by Zan⁽²⁵⁾, and with the experimental AirDyn tests of Wang *et al*⁽¹⁵⁾ and Kaaria *et al*⁽¹⁶⁾.

During a real landing manoeuvre, this loss of thrust over the flight deck during the lateral translation MTE would require the pilot to increase the collective pitch of the main rotor blades to maintain the altitude of the aircraft. This would reduce the available thrust control margin and

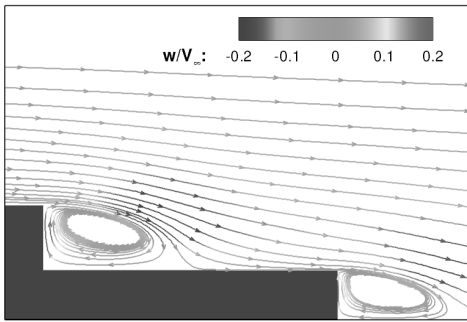


Figure 9. Mean velocity streamlines coloured by vertical velocity in the plane $y/b = 0$ for a headwind.

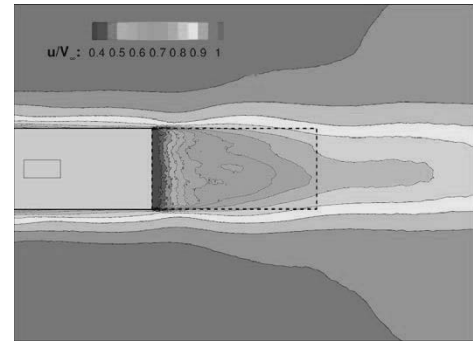


Figure 10. Contours of longitudinal mean velocity in the plane $z/h = 1.0$ for a headwind.

adversely impact the pilot's ability to respond to fluctuations in lift caused by the unsteady airwake. Reduction of the thrust control margin is a common issue associated with headwind ship deck landings, especially for low WOD speeds⁽¹²⁾.

The cause of this behaviour can be identified by studying the underlying aerodynamics of the SFS2 airwake. Figure 9 shows the time-averaged velocity streamlines over the centreline of the SFS2 flight deck for a headwind, coloured by the magnitude of the vertical velocity component. The airflow comes over the top of the hangar and reattaches to the flight deck approximately halfway along the deck, creating a significant downward component to the mean velocity of the airwake. As the helicopter translates across the flight deck, a reduction in thrust is observed because the down drafts over the deck reduce the effective angle of attack of the main rotor blades and hence the amount of thrust force produced by the main rotor. This effect is exacerbated by the reduction in longitudinal velocity experienced by the rotor disk as it passes into the recirculation region behind the hangar. Figure 10 shows contours of mean longitudinal velocity. When the helicopter model is over the deck, there will be a lower induced velocity to the main rotor blades therefore reducing the mean thrust produced.

Figure 8 shows that other longitudinal positions also exhibit the trend of decreasing mean thrust over the flight deck, although the loss of thrust is not as severe as the distance from the hangar increases. At a longitudinal position of $x/l = 0.75$, the loss of thrust is reduced as the flow is aligned more with the horizontal after reattachment (Fig. 9). At locations towards the rear of the flight deck the flow is again deflected downwards due to separation from the stern, causing a corresponding reduction in thrust.

The thrust distribution across the deck, shown in Fig. 8, is asymmetric which is again consistent with Zan's findings⁽²⁵⁾. When the helicopter is on the port side of the ship's centreline the advancing blades of the counter-clockwise rotor are in the lower velocity wake region and the retreating blades are in the higher velocity freestream region (Fig. 10). On the starboard side of the centreline the opposite is true and the advancing blades are in the higher velocity region. As a result, both the advancing and retreating blades are producing less lift at $y/b = -0.5$ than at $y/b = 0$, due to the former operating in a region of lower velocity and the latter exposed to freestream velocity. The net effect is that thrust over the starboard deck edge is approximately 4% higher than the port edge.

The time-histories in Fig. 7 also show significant fluctuations in thrust, with variations in amplitude seen between the three points. To examine this further, spectral analysis has been performed, with the resulting PSD plots shown in Fig. 11. At each of the points there is significant energy in fluctuations within the closed-loop pilot response frequency bandwidth of 0.2–2 Hz.

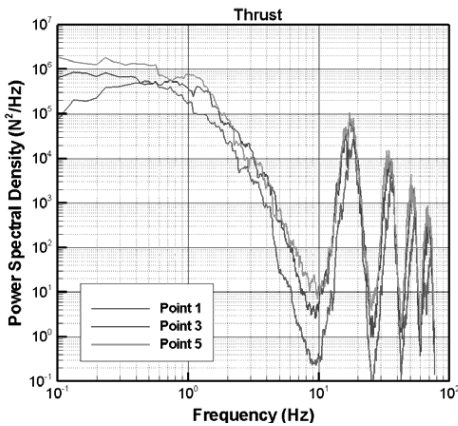


Figure 11. Power spectral density of thrust for the headwind condition at three locations relative to the flight deck.

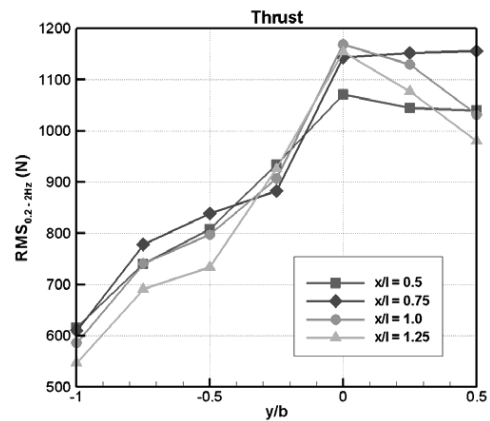


Figure 12. RMS thrust for various helicopter positions.

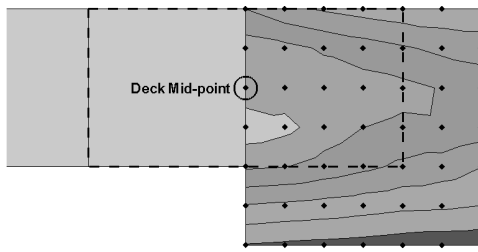
These disturbances in the thrust produced by the helicopter will impact on pilot workload as the pilot responds through the collective control to maintain a stable aircraft altitude. This control axis is particularly critical due to the aircraft's close proximity to the deck. The plots also show significant energy in disturbances at higher frequencies. These high frequency loading fluctuations, caused by the rotor harmonics, are an inherent effect of the cyclical nature of rotorcraft thrust generation. As these peaks occur at frequencies above 10 Hz they can be safely ignored in terms of pilot workload analysis, manifesting themselves as vibrations rather than disturbances which must be counteracted through pilot control inputs.

As this study is primarily concerned with the loading fluctuations in the closed-loop pilot response frequency range, the RMS thrust over this reduced bandwidth has been calculated as described earlier. Figure 12 shows RMS thrust plotted against lateral deck position for various longitudinal distances from the hangar face, which includes the three points in Figs 7 and 11. Figure 12 shows that as the aircraft translates from off the port side of the deck into the turbulent airwake over the deck, the RMS thrust increases. This is to be expected, due to the rotor being fully immersed in high levels of turbulence over the landing spot. Thus, as the pilot executes the lateral translation MTE not only will the available thrust control margin be reduced, but the workload required to maintain a stable hover altitude will increase as a result of the greater unsteadiness in the RMS thrust. The combination of these two factors is especially problematic as a reduced control margin will impact on the pilot's ability to respond to fluctuations in this axis.

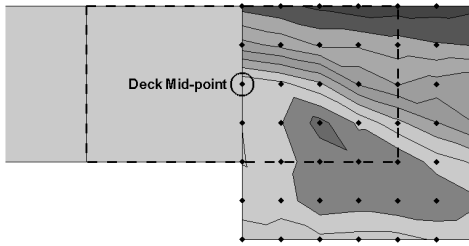
Figure 12 also shows that RMS thrust loading is asymmetric across the deck and is higher on the starboard side of the ship centreline, even though the turbulence is reasonably symmetrical across the deck for a headwind. This asymmetry is again because of the rotational direction of the main rotor where the advancing and retreating blades will react differently to the unsteady longitudinal and vertical velocity components.

4.2 Effect of wind-over-deck angle

In this section the RMS forces and moments for the headwind and G30 WOD conditions have been analysed to identify and compare their specific loading characteristics. Figure 13 shows contour plots of RMS roll moment for the two wind conditions. Greater levels of RMS roll moment are evident in the G30 case, especially towards the port side of the deck. This is because of the greater

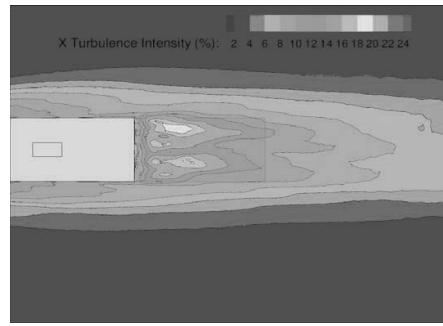


(a) headwind

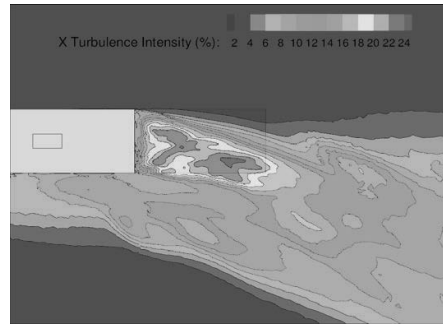


(b) Green 30

Figure 13. Contours of RMS roll moment for headwind (a) and G30 (b) WOD angle.



(a) Headwind



(b) Green 30

Figure 14. Contours of longitudinal turbulence intensity for headwind (a) and G30 (b) in the plane $z/h = 1.0$.

unsteadiness of the airwake in these regions which can be seen in the longitudinal turbulence intensity contours shown in Fig. 14.

The high levels of turbulence over the flight deck in the G30 case are caused primarily by shear layer separation from the windward top horizontal edge and vertical edge of the hangar⁽⁸⁾ which leads to the increased RMS roll moments compared with the headwind case. The increase in roll unsteadiness in the closed-loop pilot response bandwidth will increase the pilot workload required to maintain aircraft stability throughout the station-keeping MTE over the flight deck. This was also seen in the piloted flight simulation study by Forrest *et al*⁽¹⁸⁾ involving a Lynx helicopter and SFS2 airwakes, where G30 WOD conditions resulted in greater pilot workload when compared with the headwind case.

The greater roll moment unsteadiness for a G30 wind evident when the aircraft is positioned at the port side of the ship is due to the higher levels of turbulence in this region, caused by the shedding of vortical structures from the windward edge of the superstructure. This means that pilot workload during the port-side hover and lateral translation will also be greater for the G30 case. The RMS loading in the headwind case is low at the port-side approach and increases as the helicopter translates into the turbulent wake over the deck. The G30 case on the other hand has an equally significant RMS roll moment at the location of the port-side hover and along the path of the lateral translation as over the flight deck. This will cause the pilot to work hard to control the aircraft for a considerably longer time period than for a headwind landing.

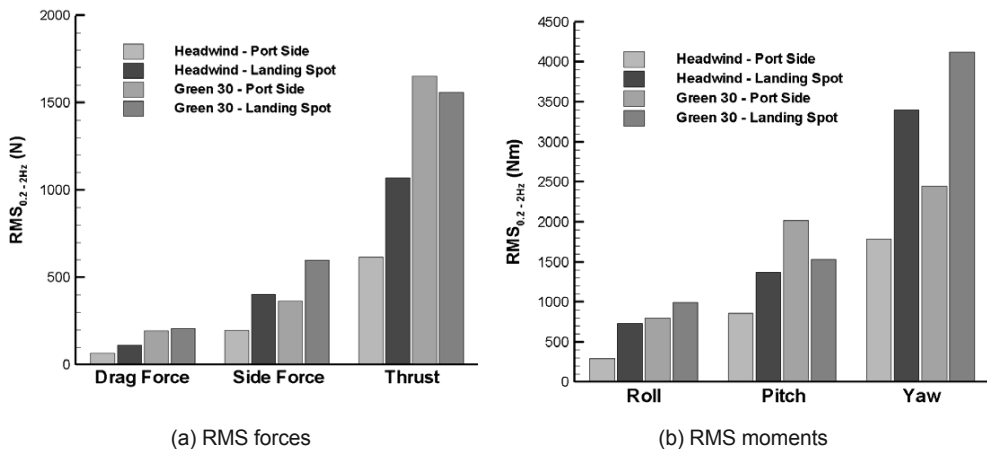


Figure 15. RMS loading comparison of forces (a) and moments (b) for the port-side and landing spot hover locations.

Figure 13 also shows that on the starboard side of the deck the RMS roll loading is greater for the headwind compared with the G30 WOD angle. This is because in the G30 case most of the main rotor and the tail rotor have moved out of the turbulent airwake into the lower turbulence, higher mean velocity, freestream region. Figure 13 shows how the RMS roll loading, in the G30 case, falls sharply after the helicopter passes the centreline of the ship towards the starboard side. In comparison, the RMS loading in the headwind case remains relatively constant across the deck due to the smaller spatial gradients of turbulence across the deck. As with the RMS thrust for the headwind case discussed earlier, the RMS roll moment is asymmetric across the deck but this time with higher values on the port side. Again this is an effect of the rotational direction of the main rotor, and possibly the configuration of the inclined SH-60B tail rotor which will affect pitch, roll and yaw characteristics.

4.3 Effect of hover position

Figure 15 shows a comparison of RMS loading for two helicopter locations: over the sea off the port side, and over the landing spot. In the headwind case, RMS loading is greater over the spot in every axis. This is because in this location the helicopter is fully immersed in the highly turbulent airwake. The unsteadiness in the airflow causes fluctuations in the aerodynamic loading and rotor response of the helicopter in the closed-loop pilot response frequency range. When the model is positioned at the port-side hover, the lower turbulence levels in the freestream have led to lower RMS loadings than over the landing spot.

Therefore, during a deck landing operation in this WOD condition, the pilot workload required to maintain a stable aircraft attitude, heading and altitude will increase as the helicopter translates over the deck to the position of the station keeping MTE. This was observed in piloted flight simulation trials conducted by Forrest *et al*⁽¹⁸⁾, where pilot comments consistently reported the highest workload to be when the helicopter was over the deck.

In the G30 case, such a clear difference in the RMS loading between the two WOD conditions does not exist. Figures 15(a) and 15(b) show that RMS loading in the side force and yaw axes is greater over the landing spot. This is because of a large unsteadiness in the lateral velocity component of the airwake in this region. This unsteadiness is caused by the flapping shear layer

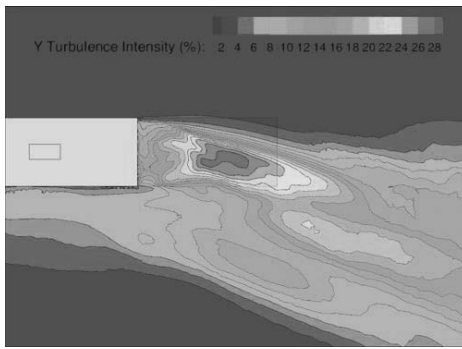


Figure 16. Contours of lateral turbulence intensity in the plane $z/h = 1.0$ for G30 WOD condition.

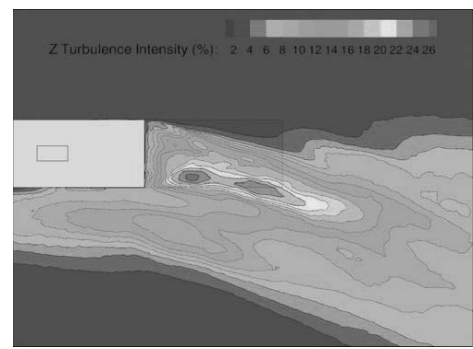


Figure 17. Contours of vertical turbulence intensity in the plane $z/h = 1.0$ for G30 WOD condition.

created as the flow separates from the windward vertical edge of the hangar⁽⁸⁾. Figure 16 shows that the greatest lateral turbulence intensity is concentrated over the flight deck. The lateral unsteadiness in the airflow leads to fluctuations in the aerodynamic loading of the fuselage and tail rotor, resulting in an RMS loading over the spot which is 40% greater than over the port side for both side force and yaw moment.

The headwind case also has a greater RMS side force and yawing moment over the spot compared with the port-side hover. As with the G30 case, the greater unsteadiness of the lateral velocity component of the airflow interacting with the fuselage and tail rotor in this region has resulted in the larger RMS loadings when the helicopter is over the spot. This suggests a link between unsteady side force and yawing moment and that these quantities are especially sensitive to the lateral turbulence of the airwake.

The ability to identify specific loading characteristics and their underlying aerodynamic causes is a key advantage of using the Virtual AirDyn. It enables airwake structures that are particularly detrimental to helicopter handling qualities to be identified along with the specific geometric features which give rise to them. Thus, ship design changes or modifications can be implemented to specifically target such features and mitigate their effects on pilot workload. For example, if a particular ship's airwake is known to cause large disturbances in the yaw axis, a clear correlation like the one drawn above would lead to ship modifications targeting the reduction of airwake lateral turbulence. The method employed in this study could then be used to assess the effect of such modifications on the unsteady yaw characteristics of a helicopter in the airwake.

Figure 15(a) shows that, in the G30 case, the unsteady thrust characteristic differs from side force and yaw in that RMS thrust is slightly greater for the port-side hover position than for over the landing spot. To identify the reasons behind this observation it is necessary to look at the vertical turbulence intensity in the airwake shown in Fig. 17. Although the longitudinal and lateral turbulence is greater in the region over the spot, Fig. 17 shows that the vertical airwake turbulence is greatest over the port edge of the deck. There is also a region of relatively high vertical turbulence intensity over the sea approximately one rotor diameter off the port side of the deck, caused by vortical structures emanating from the top windward edge of the superstructure and funnel⁽⁸⁾.

The thrust response of the helicopter is sensitive to turbulence in the vertical direction because as the vertical velocity component of the airwake fluctuates, so too will the effective angle of attack of the induced airflow to the main rotor blades and therefore the magnitude of the thrust force produced⁽²³⁾. When the helicopter is in the port-side hover position, both the advancing and

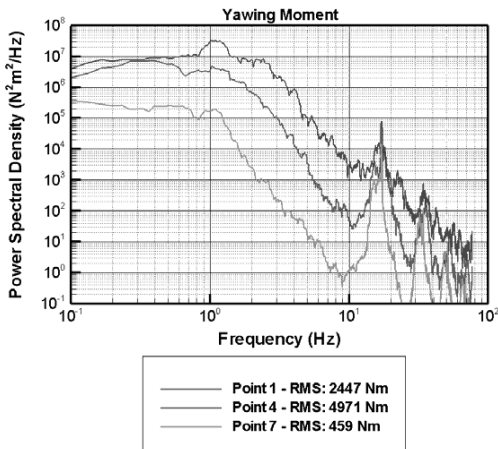


Figure 18. Power spectral density of yawing moment for G30 WOD angle at three points along $x/l = 0.5$.

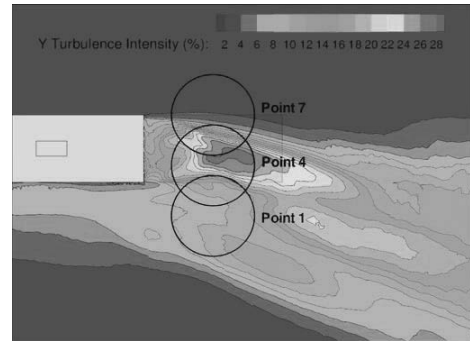


Figure 19. Contours of lateral turbulence intensity in the plane $z/h = 1.0$ and the areas swept by main rotor blades.

retreating blades are interacting with airflow containing a large vertical unsteadiness. The influence of the unsteady vertical velocity component is the principal reason behind the greater RMS thrust observed for the port-side hover location.

Figure 15(a) shows that the unsteady thrust characteristic is different for the G30 WOD condition and the headwind case discussed earlier. RMS thrust is greater in the G30 case because of the greater turbulence intensities in all three directions. However, whereas in the headwind case unsteadiness in the thrust increases as the helicopter translates over the deck, in the G30 case RMS is equally significant over the port-side hover. Larger amplitude loading fluctuations in the closed-loop pilot response frequency bandwidth seen in the G30 case will make it more difficult for the pilot to respond to disturbances and maintain aircraft stability. Therefore, the greater RMS thrust over the spot in the G30 case will enforce a greater pilot workload during both the station keeping and port-side hover MTEs. This will make a landing task much more demanding as the pilot has to work hard to maintain a stable altitude for a longer period of time.

Figure 15(b) also shows that in the G30 case the RMS pitch moment is greater at the port-side hover compared with over the spot. At this location the advancing blades of the rotor are passing through the region of high vertical turbulence intensity over the port deck edge (Fig. 17). Due to the 90° phase shift characteristic of rotor dynamics⁽²³⁾, these fluctuations in the vertical velocity component will manifest themselves as disturbances in the pitch of the aircraft. This, in turn, has resulted in the greater RMS pitching moment for the port-side hover shown in Fig. 15(b).

4.4 RMS yawing moment in G30 wind

Figure 18 shows PSD plots of yawing moment for three different lateral locations along $x/l = 0.5$. All three points show significant energy in the closed-loop pilot response frequency range, with the corresponding RMS yawing moments over this bandwidth shown in the legend. The greatest RMS yaw moment is observed when the model is at Point 4; this point has been chosen for analysis

because in this position the main and tail rotor are fully immersed in the highly unsteady region of the airwake caused by the flapping shear layer created by the flow separation from the windward vertical edge of the hangar⁽⁸⁾.

Figure 19 shows the areas swept by the main rotor blades of the model SH-60B at the three locations, superimposed onto a contour plot of lateral turbulence intensity for a G30 wind. The airflow interacting with the side of the fuselage and tail rotor blades at Point 4 is highly turbulent and leads to a large unsteadiness in the yaw moment in the closed-loop pilot response frequency bandwidth. With the main rotor positioned at Point 4, the tail rotor is over the flight deck at the rear of the ship, between points 26 and 33.

Figure 18 also shows that Point 1 has a large RMS yaw loading at G30 due to the turbulence over the port side, caused by the large scale flow structures emanating from the windward side of the superstructure⁽⁸⁾. When the helicopter model is at Point 7, over the starboard edge of the deck, most of the fuselage, main rotor and tail rotor are no longer interacting with the highly turbulent airwake and are instead immersed in the lower turbulence freestream region. This has resulted in a significantly lower RMS yawing moment at this point because of the removal of the majority of the airwake disturbances in this axis.

As the pilot translates the helicopter over the deck, a significant portion of the pilot's workload will be directed towards responding to unsteady yaw disturbances caused by the unsteady airwake. In the G30 case, the RMS yaw moment is also greatest over the flight deck where the pilot is under most pressure to maintain stable attitude and heading before any attempted descent to the landing spot. Therefore future investigations into ship superstructure modifications should focus on reducing the effects of shear layer turbulence. There are several possible methodologies that may achieve this, including the deflection of the shear layer using various configurations of inclined screens or through the 'breaking up' of airwake turbulence into higher frequency disturbances that are outside the closed-loop pilot response frequency range of 0.2-2Hz.

5.0 CONCLUSIONS

The Virtual AirDyn has been shown to be capable of measuring the aerodynamic loading imposed on a helicopter by a ship's airwake. Measurements of the mean and unsteady RMS forces and moments imposed on the helicopter have been made at various points relative to the flight deck of a simplified frigate, the SFS2, for winds coming from ahead and Green 30. The loads that have been measured are consistent with previous reports from experiments and from pilot experience.

The characteristics of the mean and unsteady loads can be explained by the underlying aerodynamic flow field which, in turn, can be associated with particular geometric features on the ship's superstructure.

The Virtual AirDyn has been shown to be a viable technique for investigating the effect of the ship's superstructure design on helicopter handling qualities and pilot workload. Future work will use the Virtual AirDyn to investigate the impact of various ship geometric features on helicopter loading to provide guidance to ship designers.

ACKNOWLEDGEMENTS

The authors are grateful to ANSYS Inc. who provided valuable assistance with the CFD. They would also like to thank Phillip Perfect from the Flight Science and Technology research group at the University of Liverpool for his guidance and expertise.

REFERENCES

1. CHENEY, B.T. and ZAN, S.J. CFD Code validation data and flow topology for the Technical Co-operation Program AER-TP2 Simple Frigate Shape, 1999, National Research Council of Canada, Report LTR-LA-294.
2. ZAN, S.J. Surface flow topology for a simple frigate shape, *Canadian Aeronautics and Space J*, 2001, **47**, (1), pp 33-43.
3. JOHNS, K.M. and HEALEY, J.V. The airwake of a DD-963 Class destroyer, *Naval Engineer's J*, 1989, **101**, (3), pp 36-42.
4. HEALEY, J.V. Establishing a database for flight in the wakes of structures, *J Aircr*, 1992, **29**, (4), pp 559-564.
5. RHOADES, M.M. and HEALEY, J.V. Flight deck aerodynamics of a nonaviation ship, *J Aircr*, 1992, **29**, (4), pp 619-626.
6. BROWNELL, C.J., LUZNIK, L, SNYDER, M.R., KANG, H.S. and WILKINSON, C.H. In situ measurements in the near-wake of a ship superstructure, *J Aircr*, 2012, **49**, (5), pp 1440-1450.
7. BARDERA MORA, R. An experimental helicopter wind envelope for ship operations, *World Academy of Science, Engineering and Technology*, 2012, **68**, pp 1362-1369.
8. FORREST, J.S. and OWEN, I. Investigation of ship airwakes using detached-eddy simulation, *Computers and Fluids*, 2010, **39**, pp 656-673.
9. THORBER, B., STARR, M. and DRIKAKIS, D. Implicit large eddy simulation of ship airwakes, *Aeronaut J*, 2010, **114**, (1162), pp 715-736.
10. POLSKY, S.A. and BRUNER, C.W. Time-accurate computational simulations of an LHA ship airwake, 2000, AIAA Paper 2000-4126, 18th Applied Aerodynamics Conference and Exhibition, August 2000 Denver, CO, USA.
11. POLSKY, S.A. A Computational study of unsteady ship airwake, 2002, AIAA Paper 2000-4126, 40th Applied Aerospace Sciences Meeting and Exhibition, 14-17 January 2002, Reno, NV, USA.
12. ZAN, S.J. On aerodynamic modelling and simulation of the dynamic interface, *Proceedings of the Institution of Mechanical Engineers, Part G: Aerospace Engineering*, 2005, **219**, pp 393-410.
13. LEE, R.G. and ZAN, S.J. Unsteady aerodynamic loading on a helicopter fuselage in a ship airwake, *J American Helicopter Society*, April 2004, **49**, 2, pp 149-159.
14. LEE, R.G. and ZAN, S.J. Wind tunnel testing of a helicopter fuselage and rotor in a ship airwake, September 2003, 29th European Rotorcraft Forum, Freidrichstrafen, Germany.
15. WANG, Y., CURRAN, J., PADFIELD, G.D. and OWEN, I. AirDyn: An instrumented model-scale helicopter for measuring unsteady aerodynamic loading in airwakes, *Meas Sci Technol*, 2012, **22**, (4), 045901.
16. KÄÄRIÄ, C.H., WANG, Y., PADFIELD, G.D., FORREST, J.S. and OWEN, I. Aerodynamic loading characteristics of a model-scale helicopter in a ship's airwake, *J Aircr*, 2012, **49**, 4, pp 1020-1031.
17. KÄÄRIÄ, C.H., WANG, Y., WHITE, M.D. and OWEN, I. An experimental technique for evaluating the aerodynamic impact of ship superstructures on helicopter operations, *Ocean Engineering*, 2013, **61**, pp 97-108.
18. FORREST, J.S., HODGE, S.J., OWEN, I. and PADFIELD, G.D. An investigation of ship airwake phenomena using time-accurate CFD and piloted helicopter flight simulation, September 2008, 34th European Rotorcraft Forum, Liverpool, UK.
19. DUVAL, R.W. A real-time multi-body dynamics architecture for rotorcraft simulation, November 2001, RAeS Flight Simulation Group Conference on The Challenge in Achieving Realistic Training in Advanced Rotorcraft Simulators, London, UK.
20. MANIMALA, B.J., WALKER, D.J., PADFIELD, G.D., VOSKUIJL, M. and GUBBLES, A.W. Rotorcraft simulation modelling and validation for control law design, *Aeronaut J*, February 2007, **111**, (1116), pp 77-88.
21. HOWLETT, J.J. UH-60A Black Hawk Engineering Simulation Program: Volume I – Mathematical model, December 1981, NASA-CR-166309.
22. BECK, C.P. and FUNK, J.D. Development and validation of a Seahawk blade element helicopter model in support of rotorcraft shipboard operations, May 1994, RAeS Rotorcraft Group Conference on Rotorcraft Simulation, London, UK.
23. PADFIELD, G.D. *Helicopter Flight Dynamics*, 2nd Edition, 2007, Blackwell.
24. McRUER, D.T. Interdisciplinary interactions and dynamic systems integration, *Int J Control*, 1994, **59**, (1), pp 3-12.
25. ZAN, S.J. Experimental determination of rotor thrust in a ship airwake, *J American Helicopter Society*, April 2002, **47**, (2), pp 100-108.